Multidiffractive Broadband Plasmonic Absorber

Imran Khan, Hamid Keshmiri, Florian Kolb, Theodoros Dimopoulos,
Emil J. W. List-Kratochvil, and Jakub Dostalek*

A novel plasmonic structure for absorbing light over broad range of wavelengths and angles of incidence is reported. It is based on a corrugated metallic grating with multiple superimposed periodical modulations for diffraction coupling of light to surface plasmons. This approach combines the advantages of regular periodic and random structures as it allows for strong as well as broadband coupling of light to surface plasmon waves. In order to demonstrate this concept, a multidiffractive structure is sequentially recorded by laser interference lithography into a photoresist, copied into an UV cross-linkable polymer, and subsequently coated by aluminum and a thin standard polymer-based photovoltaic active material layer (poly(3-hexylthiophene) (P3HT) and 1-(3-methoxycarbonyl)propyl-1-phenyl[6,6]C$_{61}$ (PCBM)). Experiments and numerical simulations are carried out in order to design a three-diffraction crossed grating corrugation for plasmonic extending of the absorption band of the P3HT:PCBM into near-infrared part of spectrum. The work demonstrates that this structure enhances the absorption in the P3HT:PCBM by a factor of 2.9 in the spectral window 600–750 nm where it is inherently weakly absorbing. Over the whole visible/NIR part of spectrum 400–750 nm the number absorbed photons in P3HT:PCBM is increased by 28%.

1. Introduction

The coupling of light to surface plasmons that originate from collective oscillations of conduction electrons at metallic surfaces allows tightly confining its energy. Such plasmonic confinement of electromagnetic field allows bridging between dimensions dictated by the sub-micrometer wavelength of light in visible and near-infrared (NIR) part of spectrum and nanoscale size of species which are often used as emitting or absorbing materials.[1] Currently, we witnessed numerous approaches to plasmonic light management in optical devices including thin film solar cells[2] and light emitting diodes.[3] In these technologies, the implemented plasmonic structures are typically designed to couple light over broad range of wavelengths and angles of incidence. For plasmonic broadband absorption of light, the majority of explored metallic structures support localized surface plasmons (LSPs). The most common approach implies a geometry consisting of metallic nanoparticles that are separated from a continuous metallic surface by a thin dielectric spacer. Such metal–dielectric–metal configurations were investigated in form of periodic arrays of rectangular and cylindrical nanoparticles[4] or nanoholes[5] and they showed the possibility to harvest light over broad range of angles of incidence. However, the resonant coupling to LSPs typically occurs only in a very narrow spectral window. In order to broaden the LSP resonance, superimposing multiple LSP resonances was investigated by stacking of nanoparticles perpendicular to the surface,[6] by arranging arrays of nanoparticles with different size in the lateral direction,[7] or by using nanostructures with more complex shapes.[5,8] Exploitation of propagating surface plasmons (PSPs) travelling along continuous metallic films was proposed for broadband absorption of light by using geometries with singularities.[9] This concept was experimentally carried out by using arrays of deep convex gold slits that were adiabatically tapered. Structures with slit tapers featuring the width as small as ≈10 nm were prepared by focused ion beam (FIB) milling and broadband absorption of light over visible and near-infrared part of spectrum was demonstrated.[10] Contrary to these, shallow periodic corrugation of metallic surfaces can be utilized by simpler means of fabrication over large areas by techniques such as laser interference lithography (LIL) or nano-imprint lithography (NIL). When coated with a metal, these structures act as gratings that can be tuned to nearly perfectly absorb light by diffraction coupling to PSPs. However, similar to LSPs, the diffraction excitation of PSPs is resonant and occurs only at narrow wavelength band which is highly sensitive to variations in the angle of incidence. In order to broaden the wavelength range where light is absorbed by diffraction coupling to PSPs, a metallic film with a periodically corrugated interface in the lateral direction was interfaced with one-dimensional photonic

I. Khan, H. Keshmiri, Dr. J. Dostalek
AIT-Austrian Institute of Technology GmbH
Biosensor Technologies
Muthgasse 11, Vienna 1190, Austria
E-mail: jakub.dostalek@ait.ac.at
I. Khan, Dr. T. Dimopoulos
AIT-Austrian Institute of Technology GmbH
Energy Department
Giefinggasse 2, Vienna 1210, Austria
F. Kolb, Prof. E. J. W. List-Kratochvil
NanoTecCenter Weiz Forschungsgesellschaft mbH
Franz-Pichler-Straße 32, 8160 Weiz, Austria
Prof. E. J. W. List-Kratochvil
Institute of Solid State Physics
Graz University of Technology
Petersgasse 16, A-8010 Graz, Austria

crystal in the direction perpendicular to the surface, generating a rich spectrum of surface plasmon-like modes.[11]

Besides periodic structures, also nonperiodic patterns were investigated for broadband collecting of light by diffraction and scattering-based coupling to optical waveguide modes and PSPs. It should be noted that the excitation and scattering of PSP on rough metallic surfaces was a subject to studies since seventies in the last century.[12] More recently we witnessed investigations on engineered randomized arrays of metallic bars[13] and dielectric pillars[14] for trapping in optical waveguides and metallic films with quasiperiodic arrays of nanoholes[15] and relief gratings[16] for the excitation of PSPs that were fabricated by electron beam lithography or FIB. Here we present a new type of broadband plasmonic absorber that relies on a periodic corrugation of metallic surface with multiple superimposed spatial frequencies. This approach allows for simultaneous diffraction coupling to PSPs at series of resonant wavelengths that span over a broad spectral range. The structures exhibit low aspect ratio features which makes them compatible with a range of thin film devices where active layers (thickness in the range of 100–200 nm) are used to emit or absorb light propagating at broad range of incident angles and wavelengths in the far field.

2. Results and Discussions

The investigated geometry consists of a metallic surface with relief corrugation profile that comprises multiple spatial frequencies. As indicated in **Figure 1**a, this corrugation was designed to simultaneously excite PSPs at a series of distinct

wavelengths. The grating was prepared by sequential LIL recording of a periodic sinusoidal interference pattern with varied period Λ into a photoresist layer. Then, this pattern was transferred to an UV-curable polymer layer by using soft lithography and such prepared replicas were subsequently coated by Al film with a thickness of $d_{Al} \approx 100$ nm and a layer of a polymer blend consisting of P3HT:PCBM with a thickness of about $d_a = 35$–40 nm. P3HT:PCBM was chosen as a model material because it is commonly used as the active material layer in polymer-based photovoltaic research.[17] This polymer blend strongly absorbs light at wavelengths around 500 nm but above the wavelength of 600 nm its absorption rapidly decreases. In order to absorb light in P3HT:PCBM more efficiently in the spectral window between 600 and 750 nm, the underneath Al surface was corrugated by a crossed grating with three encoded periods $\Lambda_1 = 535$ nm, $\Lambda_2 = 612$ nm, and $\Lambda_3 = 690$ nm as shown in Figure 1b. As described further, these periods were chosen based on the phase-matching condition in order to couple normally incident light to PSPs at the interface between Al and P3HT:PCBM. The coupling wavelengths were chosen with about 75 nm spacing in this spectral region. Fourier transform analysis of a corrugation profile cross-section that is shown in Figure 1c was used to determine amplitudes a_1, a_2, and a_3 for each recorded period Λ_1, Λ_2, and Λ_3, respectively. The obtained Fourier spectrum in Figure 1d reveals that the prepared corrugation profile exhibits distinct peaks corresponding to modulation amplitudes of $a_1 = 15.3$ nm, $a_2 = 18.5$ nm, $a_3 = 14.3$ nm. In general, superimposing of spatial frequencies leads to their mixing and thus there occur additional modulations with periods $1/(1/\Lambda_p \pm 1/\Lambda_q)$, where p and q are integers. For the
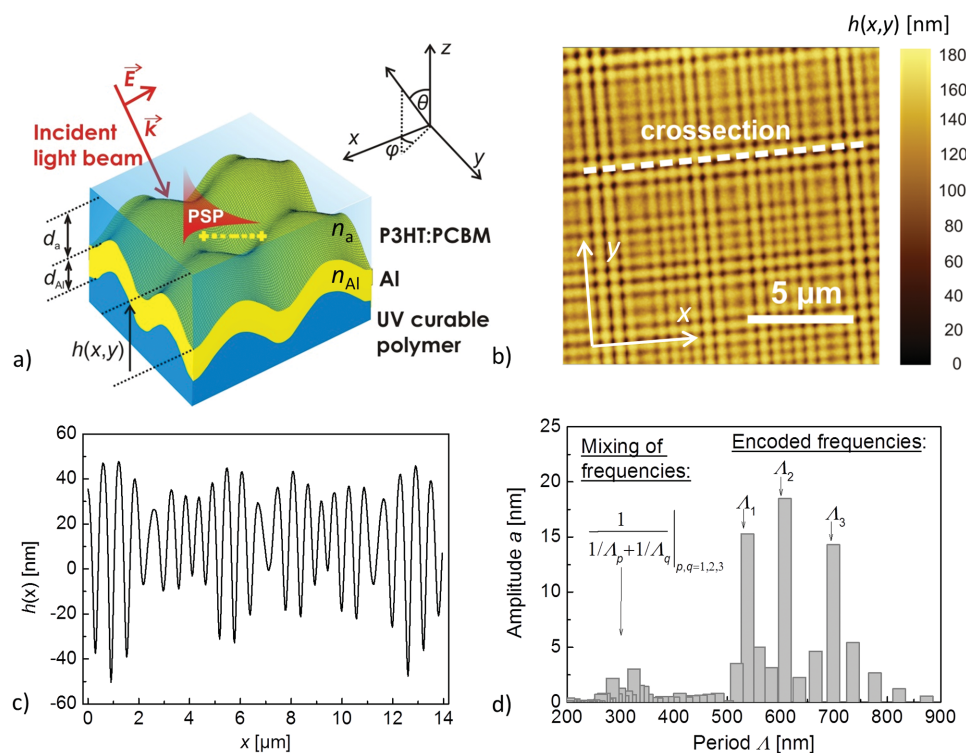
Figure 1. a) Geometry of a multidiffractive grating with Al and P3HT:PCBM layers, b) corrugation profile of 2D crossed multidiffractive grating observed with AFM, and c) cross-section of the height dependence $h(x)$ indicated as a dashed line in (b) with d) respective FFT spectrum.

selected periods Λ_1, Λ_2, and Λ_3, the subtractive frequency mixing $1/(1/\Lambda_p - 1/\Lambda_q)$ gives rise to periods Λ of several micrometers. On the other side, the additive mixing $1/(1/\Lambda_p + 1/\Lambda_q)$ is represented by series of peaks at $\Lambda = 260$–350 nm in the Fourier transform spectrum.

Relief periodic modulation of Al surface allows for diffraction coupling of far field optical waves to PSPs. On a linear 1D grating this coupling occurs when an impinging transverse magnetically polarized (TM) wave is phase-matched with PSPs by the grating momentum $2\pi/\Lambda$:

$$\pm \mathrm{Re}\{k_{PSP}\} = k_0 \sin(\theta) + m\frac{2\pi}{\Lambda} \qquad (1)$$

where θ is the angle of incidence of the incident optical beam, $k_0 = 2\pi/\lambda$ is the wavenumber of light in vacuum, m is the diffraction order, and k_{PSP} is the propagation constant of PSP modes at the Al surface. As illustrated in **Figure 2**a, the phase-matching occurs at wavelengths where the PSP dispersion relation intersects with that of diffracted light. On Al surface in contact with air (without P3HT:PCBM), normally incident light beam couples to PSPs via the first diffraction order ($m = \pm1$) at wavelengths λ between 540 and 700 nm when the grating period is tuned between $\Lambda = 535$ nm and $\Lambda = 690$ nm. The experimental data in Figure 2b reveal that on linear 1D Al grating with periods $\Lambda_1 = 535$ nm, $\Lambda_2 = 612$ nm, and $\Lambda_3 = 690$ nm and amplitudes $a_1 = 15.3$ nm, $a_2 = 18.5$ nm, and $a_3 = 14.3$ nm a polychromatic normal incident beam simultaneously excites PSPs at three distinct wavelengths of $\lambda = 540$, 630, and 700 nm. The PSP excitation manifests itself as reflectivity dips at wavelengths that agree with the values predicted by the phase-matching condition (compare with blue-marked intersections in Figure 2a). At these wavelengths, the energy of an impinging optical beam with TM polarization is transferred to PSPs and dissipates due to Ohmic losses in the metal. When increasing the polar angle of incidence θ, each resonance splits into two branches due to the plus and minus first order diffraction coupling ($m = +1$ or -1). The coupling that is associated with the additional spatial frequencies originating from mixing between Λ_1, Λ_2, and Λ_3 is not observed in the wavelength range of 400–850 nm. The reason is that respective periods are either too short (around 300 nm) or too long (several µm) and do not allow fulfilling the phase-matching condition.

After depositing P3HT:PCBM film on a flat Al surface, the reflectivity decreases in the wavelength band between 450 and 600 nm where this polymer blend exhibits strong absorption. The measured data in **Figure 3** show that when P3HT:PCBM layer is deposited on a corrugated surface of 1D three-diffraction Al grating, additional three reflectivity dips occur in the NIR part of spectrum besides the absorption band of P3HT:PCBM. These dips are associated with the resonant coupling to PSPs at wavelengths that are red shifted with respect to those observed on the Al surface in contact with air (as indicated in simulations presented in Figure 2a by red circles). The reason is that the polymer layer exhibits large real part of the refractive index $\mathrm{Re}\{n_a\}$ which increases the PSP propagation constant $\mathrm{Re}\{k_{PSP}\}$. The three resonances occur at wavelengths $\lambda = 635$, 685, and 750 nm which is in the spectral region where P3HT:PCBM exhibits small imaginary part of refractive index ($\mathrm{Im}\{n_a\} = 0.16$
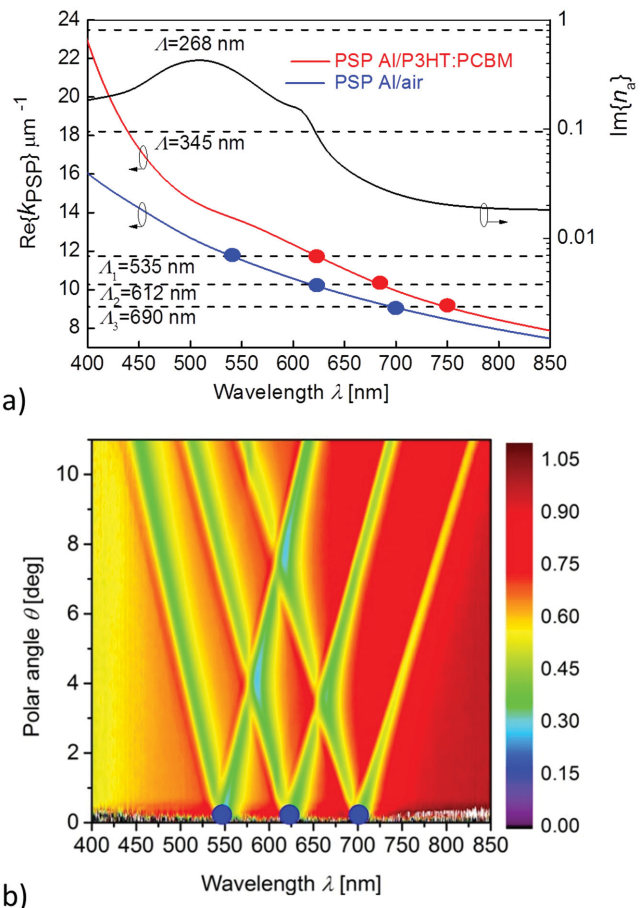
Figure 2. a) Diffraction phase matching of PSP dispersion relation on Al surface without (blue line) and with (red line) the P3HT:PCBM layer. Polymer layer thickness is of $d_a = 40$ nm. For comparison, the imaginary part of P3HT:PCBM refractive index $\mathrm{Im}\{n_a\}$ is shown. b) Measured dependence of TM specular reflectivity on polar angle θ and wavelength λ for 1D three-diffraction Al grating without P3HT:PCBM layer. The specular reflectivity from the corrugated surface was normalized with that measured on a flat Al surface in contact with air. Modulation amplitudes for corrugated surface are $a_1 = 15.3$ nm, $a_2 = 18.5$ nm, and $a_3 = 14.3$ nm and periods $\Lambda_1 = 535$ nm, $\Lambda_2 = 612$ nm, and $\Lambda_3 = 690$ nm. The plane of incidence is defined by x and z axis (with $\phi = 0$).

at $\lambda = 600$ nm 0.02 at $\lambda = 750$ nm was measured by ellipsometry as seen in Figure 2a) and thus it only weakly absorbs. One can see that the simultaneous coupling to these three PSP modes at the Al interface efficiently extends the absorption on the surface in the selected wavelength range $\lambda = 600$–750 nm. The coupling strength to PSPs can be controlled by tuning the modulation amplitude a at each period Λ. In order to demonstrate this, three samples with amplitudes a_1, a_2, and a_3 between 0 and 10 nm were prepared and coated with Al and P3HT:PCBM polymer layers (see table in Figure 3f). Measured specular reflectivity spectra in Figure 3b,c reveal that the resonance dips associated to PSP diffraction coupling by Λ_1, Λ_2, and Λ_3 appear for weakly modulated surfaces at wavelengths predicted by the phase-matching condition (compare with Figure 2a). For deeper grating presented in Figure 3d, the resonances are slightly red shifted which can be attributed to changes in the propagation constant of k_{PSP} caused by the curved Al interface. In addition,

FULL PAPER
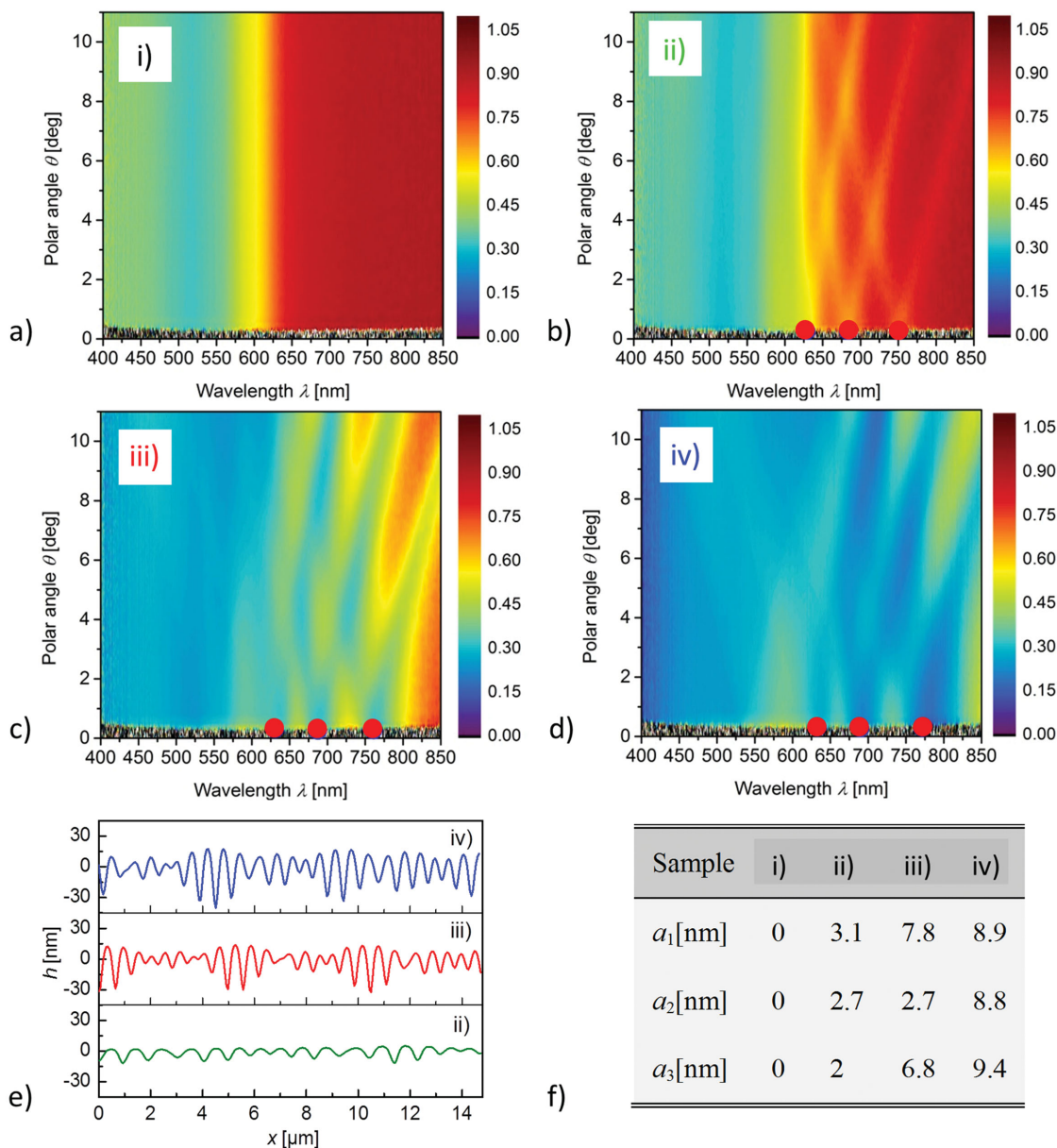
Figure 3. a–d) Measured specular TM reflectivity from 1D three-diffractive gratings for increasing modulation depth as showed in e) respective corrugation cross-sections. f) Overview of determined corrugation amplitudes of modulations at periods Λ_1, Λ_2, and Λ_3. The Al surface was coated with a 35–40 nm thick layer of P3HT:PCBM. The plane of incidence is defined by x and z axis ($\phi = 0$).

variations in the thickness of P3HT:PCBM layer occur on the stronger corrugated surface leading to a nonconformal geometry (AFM observations showed that the polymer preferably filled the grating valleys leading to the surface with substantially weaker corrugation at the polymer:air interface).

The previously discussed data were measured on linear 1D gratings with a light beam that is TM polarized. For such geometry, the orthogonal transverse electrically (TE) polarized light beam does not couple to PSPs and is reflected similar to flat layers shown in Figure 3a. In order to achieve strong broadband plasmonic absorption for both polarizations, a crossed 2D grating with a three-diffraction profile was prepared and coated with Al and P3HT:PCBM layers.

Diffraction then occurs via grating momenta in both orthogonal x (indexed with m) and y (index with n) directions and the phase-matching condition can be expressed by using polar θ and azimuthal ϕ angles as

$$\mathrm{Re}\{k_{PSP}\}^2 = \left[k_0 \sin(\theta)\cos(\phi) + m\frac{2\pi}{\Lambda} \right]^2 + \left[k_0 \sin(\theta)\sin(\phi) + n\frac{2\pi}{\Lambda} \right]^2 \tag{2}$$

As can be seen in **Figure 4**a,b, pronounced SPR dips occur both in TM and TE specular reflectivity wavelength spectrum due to the simultaneous diffraction coupling by periods Λ_1,

www.MaterialsViews.com

ADVANCED
OPTICAL
MATERIALS
www.advopticalmat.de

FULL PAPER
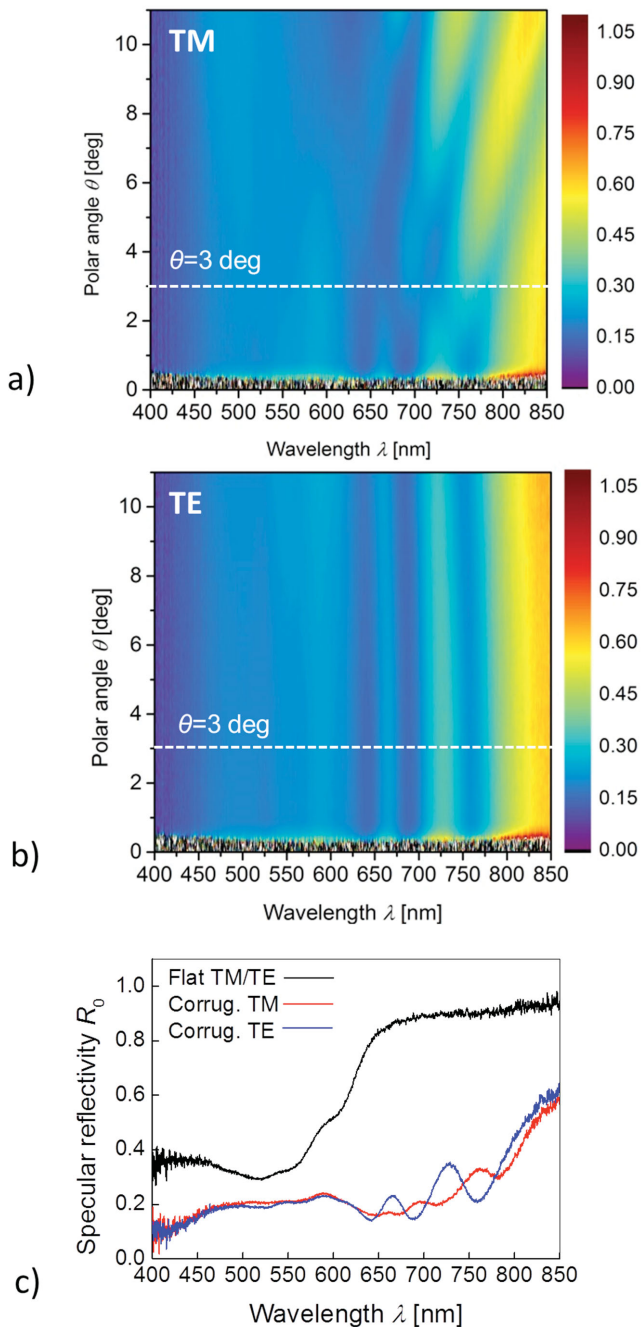
Figure 4. Measured a) TM and b) TE specular reflectivity from a 2D (crossed) three-diffractive grating with Al and P3HT:PCBM layers (profile shown in Figure 1b–d and the thickness of polymer blend was d_a = 35–40 nm). c) Cross-section of the specular reflectivity R_0 for a fixed angle of θ = 3° and azimuthal angle ϕ.

dependence of specular reflectivity R_0 in Figure 4c compares the spectra measured on flat and corrugated Al surfaces for the polar angle θ = 3° and azimuthal angle ϕ = 0. As the polar angle θ is close to zero, reflectivity curves measured for TM and TE polarization are similar because the structure is symmetrical and thus polarization insensitive at normal incidence. The small difference between TE and TM reflectivity curves can be explained by the effect of resonance splitting due to slightly deviated angle θ.

In the wavelength range of 650–750 nm more than 90% of light intensity is reflected from P3HT:PCBM layer on the top of a flat Al surface. However, the specular R_0 drops to less than 30% when the Al interface is corrugated by the developed crossed 2D grating. It should be noted that besides the specular reflection also coupling of the incident light wave to other nonspecular waves occurs via propagating diffraction orders below critical wavelengths associated with recorded periods Λ_1, Λ_2, and Λ_3 as well as due to the mixing of spatial frequencies. In order to evaluate this effect, total reflectivity was measured for a fixed angle of incidence θ = 13° by using an integration sphere and it was compared to the specular reflectivity at the same angle θ (data are presented in Figure S1 in the Supporting Information). This study showed that for long wavelengths >800 nm the specular reflectivity R_0 and total reflectivity are similar. However, at short wavelengths the diffraction competes with specular reflection and it becomes more pronounced. At wavelength of λ = 500 nm around 20% of light intensity is scattered to propagating diffraction orders on crossed multidiffractive grating.

Measured reflectivity curves were compared to finite difference time domain (FDTD) simulations. For simplicity, these simulations were carried out for 1D linear grating geometry with three superimposed periodic modulations with Λ_1 = 544 nm, Λ_2 = 618 nm, and Λ_3 = 680 nm. It should be noted that these values only approximate the periods used in the experiment and differ by <10 nm. In principle, better match can be achieved by using a larger unit cell in simulations however for the price of increased computation power required. As the width of SPR bands is typically larger than 10 nm we assume that this deviation from experiment does not change obtained results substantially.

Simulated reflectivity curves for the polar angle of incidence θ = 0 and TM polarization are presented in **Figure 5**a. They show that each modulation is associated with a distinct SPR dip at resonant wavelengths of λ = 635, 680, and 730 nm. Similar to experiments, superimposed SPR dips are associated with stronger absorption when increasing the modulation amplitudes a_1–a_3 and data for modulation amplitudes a_{1-3} = 20 nm qualitatively matches those observed experimentally in Figure 4. Besides the first order coupling to PSPs via diffraction on individual periods Λ_{1-3}, the three-diffraction Al grating with the P3HT:PCBM absorber also scatters the incident light beam to other diffraction orders propagating to the far field. This phenomenon is particularly associated with the presence of long periods originating from subtractive mixing of encoded spatial frequencies Λ_{1-3} and is more pronounced at short wavelengths below the recorded periods. Similar to observed experiments, this scattering leads to a decreased reflectivity below the wavelength 500 nm for both TM and TE polarization. In

Λ_2, and Λ_3 and orders (m,n) = (±1,0) and (0,±1). For TM polarized light and an azimuthal angle of ϕ = 0, SPR dips split when increasing the angle of incidence θ as the coupling occurs via diffraction orders (±1,0) similar as for the 1D linear grating. However, the resonant wavelengths only weakly change with θ for the TE polarized light that couples to via a grating vector perpendicular to the plane of incidence (0, ±1). The wavelength

FULL PAPER

Figure 5. a) TM specular reflectivity R_0 calculated for a light beam normally incident ($\theta = 0°$) on a three-diffractive grating with varied amplitudes a ($a_1 = a_2 = a_3$) and periods $\Lambda_1 = 544$ nm, $\Lambda_2 = 618$ nm, and $\Lambda_3 = 680$ nm. b) Near field distribution of electric field intensity $|E/E_0|^2$ for resonant wavelength $\lambda = 620$, 680, and 740 nm for amplitudes $a_{1-3} = 30$ nm.

addition, TM polarized wave can couple to PSP at wavelengths $\lambda = 400–450$ nm by periods below 345 nm that originate from additive mixing of spatial frequencies as indicated in the phase-matching diagram in Figure 2a. The simulations suggest that the diffraction coupling to PSPs on the multidiffractive grating is not sensitive to variations in phase Φ_{1-3} between encoded periodic modulations Λ_1, Λ_2, and Λ_3 which agrees with presented experimental results (in which these parameters were random and not controlled). Figure 5b shows the near field distribution of electric field intensity $|E/E_0|^2$ normalized with that of the incident beam. It reveals that the coupling to PSPs is associated with enhanced field strength on the surface with absorber layer. Interestingly, the dependence of field strength $|E/E_0|^2$ on the lateral coordinate x exhibits an envelope that peaks at different lateral areas for each resonant wavelength.

The decreased specular (zero order) reflectivity R_0 is accompanied with dissipation of light intensity in Al due to Ohmic
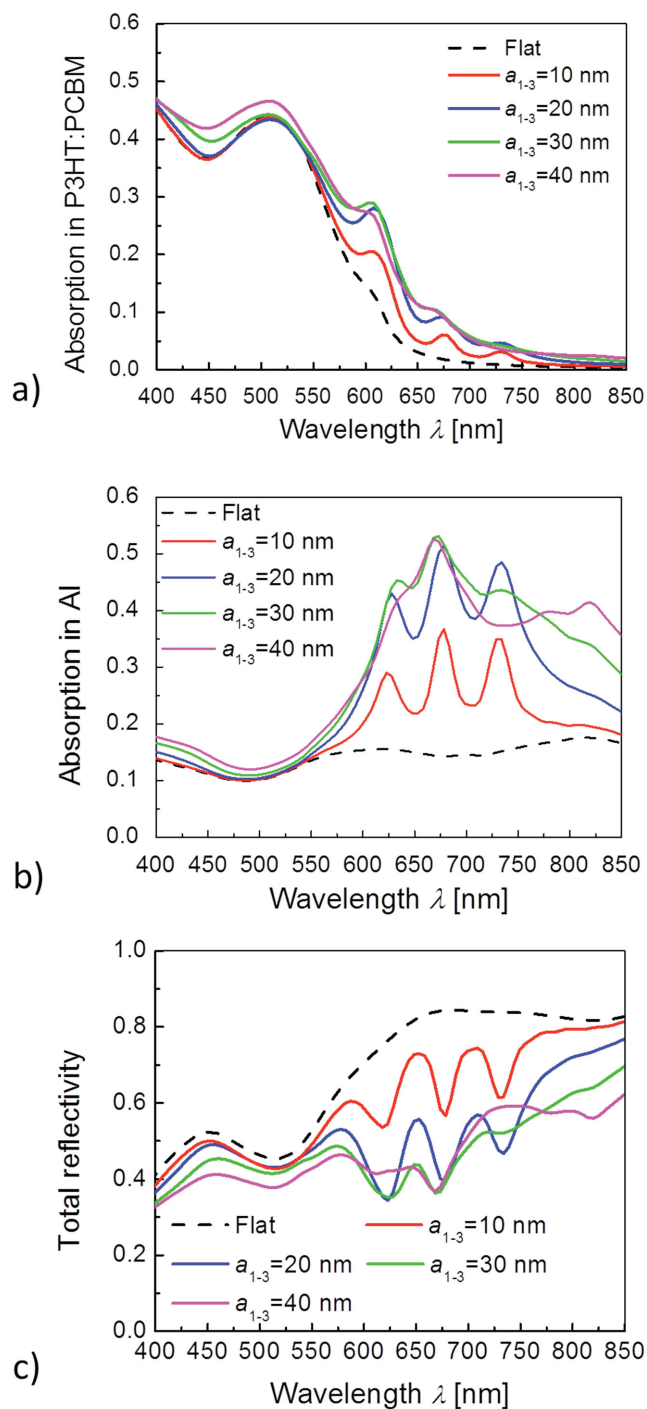
Figure 6. Simulated wavelength dependence of absorption in a) P3HT:PCBM and b) in Al layers compared to c) total reflectivity. There was assumed a TM polarized light wave normally incident at a 1D three-diffractive grating with periods $\Lambda_1 = 544$ nm, $\Lambda_2 = 618$ nm, and $\Lambda_3 = 680$ nm. Modulation amplitudes were varied between $a_{1-3} = 0$ and 40 nm as indicated.

losses, absorption in the P3HT:PCBM, or increased scattering to diffraction orders propagating to the far field. Simulations presented in **Figure 6** were carried out in order to elucidate contributions of these three processes. The absorption in

www.MaterialsViews.com

ADVANCED
OPTICAL
MATERIALS
www.advopticalmat.de

FULL PAPER

P3HT:PCBM layer in Figure 6a was simulated for the modulation amplitudes of a_{1-3} = 0–40 nm. These data reveal that substantial fraction of light energy that is trapped by PSPs is subsequently absorbed in the P3HT:PCBM layer. Interestingly, strong absorption occurs despite the fact that PSPs at Al surface penetrate to a distance of about 200 nm from the Al surface which is much longer than the thickness of the P3HT:PCBM absorber d_a. Without the corrugation (a_{1-3} = 0 nm), the absorption in P3HT:PCBM decreases with the wavelength from 15% at λ = 600 nm to 1% at λ = 750 nm. For the modulation amplitudes a_{1-3} = 20 nm, the absorption in the polymer blend is increased in this region about 1.9-times at wavelength of λ = 620 nm and by 5-times at λ = 740 nm. The wavelength dependence of absorption that takes place in Al is presented in Figure 6b and it reveals that Ohmic losses strongly compete with the absorption in P3HT:PCBM. On a planar surface, the dependence is relatively flat and about 15% of light intensity is absorbed by Al. When the surface is corrugated, this absorption increases to 35%–50% upon the resonant coupling to PSPs. Lastly, the total reflectivity (that takes into account zero order reflectivity and scattering to higher reflection orders) oscillates between 30% and 60% and it reaches its minimum when the light beam resonantly couples to PSPs. Assuming AM1.5 spectrum of incident light, the flat P3HT:PCBM layer with as small thickness as d_a = 35 nm absorbs only 4.8% of photons in the wavelength range of λ = 600–750 nm. This yield is increased by a factor of 2.9 to 14% when the Al surface is corrugated by the discussed multidiffractive profile. The performed simulations predict that this advancement translates to increased number of absorbed photons by 28% in the wider wavelength range of visible and NIR light of λ = 400–750 nm. It should be noted that major limitation in this approach represents the Ohmic losses in Al. This limitation can be overcome by using other noble metals such as Ag and Au which exhibit lower damping or by using broader spectrum of dielectric waveguide modes supported by systems with thicker layers such as those used in realistic solar cells.

Let us point out that the chosen geometry demonstrating the enhanced absorption in a thin P3HT:PCBM layer differs from those used in solar cell devices. In the presented work, we chose a thin absorber layer in order to simplify the analysis of the presented concept as then PSPs are the only guided modes on the surface that can be used for the trapping of light. Thin film PV solar cells typically rely on absorber layers with thickness d_a = 100–200 nm and then the layer structure supports additional waveguide modes. Indeed, the concept of enhancing absorption by multidiffractive grating can be adopted for these waveguide modes as well and it can offer the advantage of smaller losses associated with the attenuation in metal.

Finally, let us discuss the fact that micro/nanostructuring that enhances light absorption in the absorber does not necessarily translate to an improvement of the overall photovoltaic (PV) solar cell performance. In general, this is not an issue for aperiodic nanostructures [18] and periodic microstructures [19] that are separated from active layers of a solar cell by a transparent substrate. However, when high aspect ratio metallic nanostructures are deployed between electrodes that directly interface with solar cell absorber layer, electric field becomes modulated along the surface which can deteriorate charge carrier extraction and eventually cancel the positive effect of enhanced absorption.[20] It is therefore underlined that the impact of light management architecture that increases absorption should be at least neutral to the electrical charge transport process. The multidiffractive gratings investigated in the present work exhibit relatively shallow topographic profile. Therefore, they are not expected to cause significant electric field inhomogeneities that would hinder charge carrier harvesting. Recent investigations reported on the using of randomly attached Ag nanoparticles[21] and aperiodic relief nanostructures on Al[18] electrode in thin film plasmonic solar cells. They comprised features with feature size comparable to the present work and they were demonstrated to significantly enhance power conversion efficiency (PCE) by the increased light absorption. Ag[22] and Al[23] electrodes with relief periodic gratings were developed to advance PCE of polymer solar cell through a combination of enhanced scattering and coupling to optical waveguide modes and PSPs. Similar effects were achieved by periodically patterned Au electrode in the field of rapidly progressing perovskite solar cell technology.[24] The herein presented approach based on multidiffractive plasmonic absorber is generic and it holds potential to combine advantages of random and periodic structures for light harvesting in a wide range of thin film PV solar cells.

3. Conclusions

A new approach to broadband plasmonic absorber is proposed. It takes advantage of the coupling to surface plasmons on a multidiffractive metallic grating that provides access to tunable and rich spectrum of momenta for their phase matching with incident light. The concept was demonstrated for a thin P3HT:PCBM polymer layer on the top of a corrugated Al surface. The presented work showed that superimposing three diffraction gratings allows extending the absorption band of applied polymer blend into the NIR part of spectrum. Investigated structures can be easily prepared over large surface areas by sequential recording into a photoresist by means of laser interference lithography and multiple copies can be made by soft lithography. The presented approach is generic and can be adapted for other parts of electromagnetic field spectrum and other types of guided waves. In principle, arbitrary number of spatial frequencies can be encoded to the surface, increasing the wavelength range where the proposed plasmonic absorber is desired to trap energy of incident light. We believe that the presented approach may offer attractive means for improving performance of thin film solar cells and it can potentially find its applications for efficient extraction of light and control of angular distribution for devices such as light emitting diodes.

4. Experimental Section

Preparation of Multidiffractive Gratings: The multidiffractive grating structures were recorded by UV laser interference lithography with Lloyd's mirror configuration into the positive photoresist Microposit S1805 from Microchem (USA). First, a photoresist layer was spun onto a BK7 glass substrate at 4500 rpm for 45 s, yielding a thickness of 400 nm. Then, a soft baking step on a hot plate at 98 °C was applied for 120 s. Afterward, the substrate was mounted to the laser interference setup

and exposed to the field of collimated interfering beams (with intensity of 32 μW cm^{-2}) emitted from a HeCd laser (model IK 3031 R-C from Kimmon) at wavelength λ = 325 nm. The angle of the interfering beams was set to 17.68°, 15.39°, and 13.62° which corresponds to periods of Λ_1 = 535, Λ_2 = 612, and Λ_3 = 690 nm, respectively. In order to record a multidiffractive structure, the photoresist layer was sequentially exposed to the interference field at each respective angle for 95 s. For the preparation of crossed gratings, the sequential exposure to interference fields was carried out twice for two orientations of the sample rotated by 90°. The relief corrugation was etched into the photoresist by a developer AZ 303 from MicroChemicals (Germany) that was diluted by distilled water at a ratio of 1:15. Development time was changed in order to control the modulation depth and was typically set to ≈25 s. Prepared photoresist grating was casted to polydimethylsiloxane (PDMS) Sylgard 184 from Dow Corning (USA), followed by a curing step for 3 d at room temperature. The PDMS replica was detached from the master and employed as a working stamp. UV-curable polymer Amonil MMS 10 from AMO Gmbh (Germany) was spun on a cleaned BK7 glass substrate at 2000 rpm for 120 s which results in a layer thickness of 121 ± 5 nm. Then, the PDMS stamp was placed on the top of fluid Amonil layer which was subsequently irradiated by UV light (UV lamp Bio-Link 365 from Vilber Lourmat with the wavelength λ = 365 nm). The irradiation dose was set to 5 J cm^{-2}. Finally, the PDMS stamp was detached from the cured Amonil MMS 10, leaving a copy of the master structure in the polymer layer. The obtained multidiffractive grating structure was coated with 100 nm of Al by sputtering (UNIVEX 450C from Leybold Systems, Germany). It should be noted that each sample comprised an area that was structured and an area that was flat and served as a reference in the optical measurements.

Absorber Layer P3HT:PCBM: Regioregular poly(3-hexylthiophen-2,5-diyl) (P3HT) with a molecular weight M_W = 25–45 kDa and the fullerene derivative [6,6]-phenyl-C$_{61}$-butyric acid methyl ester (PCBM) were obtained from Sigma-Aldrich and used without further purification. Both polymer materials were dissolved in chlorobenzene in a ratio of 1:1 and stirred at temperature of 70 °C for 3 h. To ensure a complete dissolution of P3HT and PCBM, the polymer blend was stirred for an additional 15 h at room temperature. For the ellipsometric measurements, SiO$_x$ substrates were cleaned by sequentially immersing them in acetone, ethanol, and deionized water for 15 min each. Further preparation steps were carried out inside a glovebox under an inert Ar atmosphere to avoid oxygen and water induced degradation and contamination. P3HT:PCBM blend (60 g L^{-1}) was spun at 1200 rpm for 120 s and afterward heat treated at temperature of 150 °C for 15 min in order to start crystallization and diffusion processes of P3HT and PCBM, respectively. The final film thickness was found to be 350 nm, which has been estimated by AFM (Dimension V, *Veeco Digital Instruments*) operated in tapping mode, at a scratch in the film. Optical constants were determined by a variable angle spectroscopic ellipsometer from J.A. Woollam Co. Inc. (USA), in the spectral range between 300 and 1200 nm with a data step size of 10 nm and at incident angles of 65° and 75°. Analysis of obtained measurement data was done by the commercially available WVASE software application. A Gaussian oscillator model was utilized for the fitting procedure, that has been further improved by treating the investigated film as graded index layer, comprising of five different sublayers and a linear grading profile. Surface roughness of the thin film as well as an anisotropic model have not been taken into account during fitting of measurement data. For the demonstration of plasmonic multidiffractive absorber, identical protocol was used and the P3HT:PCBM polymer blend (9 g L^{-1}) was spun onto the multidiffractive grating structure coated with 100 nm of Al at 1200 rpm for 120 s. After the thermal annealing at 150 °C for 15 min, the thickness of prepared polymer film of d_a = 35–40 was determined on a reference flat glass substrate.

Reflectivity Measurement: The optical system used for the specular reflectivity measurements consisted of a white light source (halogen lamp from LSH102 from LOT-Oriel) that was connected to an optical fiber M25L02 from Thorlabs (UK). The light emitted from the optical fiber tip was collimated by an achromatic lens 14 KLA 001 CVI from Melles Griot (Germany). This collimated light beam was made incident through a polarizer at the grating sample, mounted on a motor-controlled 2θ rotation stage from Huber GmbH (Germany). One motor was used for the control of the polar angle of incidence θ, while the second motor was employed for rotating the optics collecting the reflected light beam. Reflected light beam was coupled by the collimator F810SMA-635 from Thorlabs (UK) into an optical fiber M26L02 from Thorlabs (USA) that was connected to a spectrometer HR4000 from Ocean Optics (USA). Data acquisition and system control was performed by a software developed in LabVIEW from National Instruments (USA).

Simulations: Multidiffractive grating was theoretically analyzed by using FDTD simulations implemented by Lumerical Inc. (Canada). Relief profile of a grating was defined as a superposition of periodical modulations with spatial frequencies defined as multiples of that corresponding to "superperiod" Λ. The corrugation was described by the function $h(x) = a_1\sin(2\pi k/\Lambda x + \Phi_1) + a_2\sin(2\pi l/\Lambda x + \Phi_2) + a_3\sin(2\pi m/\Lambda x \ \Phi_3)$, where a_i and Φ_i is amplitude and phase of ith modulation, respectively, and k, l, and m are integers. The superperiod was chosen to be Λ = 13.6 μm in the presented simulations and periods of three superimposed modulations were defined by the coefficients k = 25, l = 22, and m = 20 which correspond to $\Lambda_1 = \Lambda/25$ = 544 nm, $\Lambda_1 = \Lambda/22$ = 618 nm, and $\Lambda_1 = \Lambda/20$ = 680 nm. A plane optical wave was assumed to be incident at the grating with the plane of incidence defined by x and z axis. A unit cell with the width equal to the period Λ was defined and periodic boundary conditions in x axis were used. In the z direction, perfect matched layer (PML) was placed and a metal boundary condition was applied at the distances of 1 and 0.7 μm above and below the layer stack, respectively. A reflectivity monitor was placed behind the source in order to calculate the reflectivity of the structure. For simulating the near field distribution through the layer structure, there was employed a line monitor oriented along the y axis. A group of monitors consisting of the refractive index and power monitors were also used in the x–y plane in order to gather data that were further post processed by using script code which calculates the absorbed power in each layer. The dissipation in the absorber and Al was simulated by the integration of a function $\omega \mathrm{Re}\{n_x\}\mathrm{Im}\{n_x\}|E|^2$ over the volume of the layer in the unit cell, where ω is the angular frequency and n_x states for refractive index of absorber n_a or refractive index of aluminum n_{Al}. The spectrum of PSP modes supported by the investigated structure was calculated by using the model CAMFR[25] that relies on the eigenmode expansion method. Perfect matched layers were placed at the distance of 8 μm above the Al surface and 1 μm below the Al surface and the propagation constant k_{PSP} was solved. Refractive indices of Al was taken from literature [26] and the presence of thin oxide layer was omitted.

Supporting Information

Suporting information is available from Wiley Online Library or from the author.

[1] a) V. Giannini, A. I. Fernandez-Dominguez, S. C. Heck, S. A. Maier, *Chem. Rev.* **2011**, *111*, 3888; b) S. Linic, P. Christopher, D. B. Ingram, *Nat. Mater.* **2011**, *10*, 911.

www.MaterialsViews.com

ADVANCED
OPTICAL
MATERIALS
www.advopticalmat.de

FULL PAPER

[2] K. R. Catchpole, A. Polman, *Opt. Express* **2008**, *16*, 21793.

[3] G. Lozano, D. J. Louwers, S. R. K. Rodriguez, S. Murai, O. T. A. Jansen, M. A. Verschuuren, J. G. Rivas, *Light-Sci. Appl.* **2013**, *2*, e66.

[4] a) N. Liu, M. Mesch, T. Weiss, M. Hentschel, H. Giessen, *Nano Lett.* **2010**, *10*, 2342; b) A. Cattoni, P. Ghenuche, A. M. Haghiri-Gosnet, D. Decanini, J. Chen, J. L. Pelouard, S. Collin, *Nano Lett.* **2011**, *11*, 3557.

[5] C. G. Hu, L. Y. Liu, Z. Y. Zhao, X. N. Chen, X. G. Luo, *Opt. Express* **2009**, *17*, 16745.

[6] J. Q. Wang, C. Z. Fan, P. Ding, J. N. He, Y. G. Cheng, W. Q. Hu, G. W. Cai, E. J. Liang, Q. Z. Xue, *Opt. Express* **2012**, *20*, 14871.

[7] L. Wen, F. H. Sun, Q. Chen, *Appl. Phys. Lett.* **2014**, *104*, 151106.

[8] Z. H. Jiang, S. Yun, F. Toor, D. H. Werner, T. S. Mayer, *ACS Nano* **2011**, *5*, 4641.

[9] A. Aubry, D. Y. Lei, A. I. Fernandez-Dominguez, Y. Sonnefraud, S. A. Maier, J. B. Pendry, *Nano Lett.* **2010**, *10*, 2574.

[10] T. Sondergaard, S. M. Novikov, T. Holmgaard, R. L. Eriksen, J. Beermann, Z. H. Han, K. Pedersen, S. I. Bozhevolnyi, *Nat. Commun.* **2012**, *3*, 965.

[11] a) A. S. Hall, M. Faryad, G. D. Barber, L. Liu, S. Erten, T. S. Mayer, A. Lakhtakia, T. E. Mallouk, *ACS Nano* **2013**, *7*, 4995; b) L. Liu, M. Faryad, A. S. Hall, G. D. Barber, S. Erten, T. E. Mallouk, A. Lakhtakia, T. S. Mayer, *J. Nanophotonics* **2015**, *9*, 093593.

[12] H. Reather, *Surface Plasmons on Smooth and Rough Surfaces and on Gratings*, Vol. *111*, Springer-Verlag, Berlin **1983**.

[13] R. A. Pala, J. S. Q. Liu, E. S. Barnard, D. Askarov, E. C. Garnett, S. Fan, M. L. Brongersma, *Nat. Commun.* **2013**, *4*, 2095.

[14] E. R. Martins, J. T. Li, Y. K. Liu, V. Depauw, Z. X. Chen, J. Y. Zhou, T. F. Krauss, *Nat. Commun.* **2013**, *4*, 2665.

[15] a) A. E. Ostfeld, D. Pacifici, *Appl. Phys. Lett.* **2011**, *98*; 113112; b) P. W. Flanigan, A. E. Ostfeld, N. G. Serrino, Z. Ye, D. Pacifici, *Opt. Express* **2013**, *21*, 2757.

[16] I. Dolev, M. Volodarsky, G. Porat, A. Arie, *Opt. Lett.* **2011**, *36*, 1584.

[17] M. Graetzel, R. A. J. Janssen, D. B. Mitzi, E. H. Sargent, *Nature* **2012**, *488*, 304.

[18] J. D. Chen, C. H. Cui, Y. Q. Li, L. Zhou, Q. D. Ou, C. Li, Y. F. Li, J. X. Tang, *Adv. Mater.* **2015**, *27*, 1035.

[19] a) J. D. Myers, W. R. Cao, V. Cassidy, S. H. Eom, R. J. Zhou, L. Q. Yang, W. You, J. G. Xue, *Energy Environ. Sci.* **2012**, *5*, 6900; b) S. Esiner, T. Bus, M. M. Wienk, K. Hermans, R. A. J. Janssen, *Adv. Energy Mater.* **2013**, *3*, 1013; c) M. Mariano, F. J. Rodriguez, P. Romero-Gomez, G. Kozyreff, J. Martorell, *Sci. Rep.* **2014**, *4*, 4959.

[20] Y. C. Liu, C. Kirsch, A. Gadisa, M. Aryal, S. Mitran, E. T. Samulski, R. Lopez, *J. Phys. D: Appl. Phys.* **2013**, *46*, 024008.

[21] C. J. An, H. W. Yoo, C. Cho, J. M. Park, J. K. Choi, M. L. Jin, J. Y. Lee, H. T. Jung, *J. Mater. Chem. A* **2014**, *2*, 2915.

[22] J. B. You, X. H. Li, F. X. Xie, W. E. I. Sha, J. H. W. Kwong, G. Li, W. C. H. Choy, Y. Yang, *Adv. Energy Mater.* **2012**, *2*, 1203.

[23] K. Li, H. Y. Zhen, Z. Y. Huang, G. L. Li, X. Liu, *ACS Appl. Mater. Interfaces* **2012**, *4*, 4393.

[24] M. Long, Z. Chen, T. Zhang, Y. Xiao, X. Zeng, J. Chen, K. Yan, J. Xu, *Nanoscale* **2015**, DOI: 10.1039/c5nr05042a.

[25] P. Bienstman, R. Baets, *Opt. Quantum Electron.* **2001**, *33*, 327.

[26] *Handbook of Optical Constants of Solids* (Ed: E. D. Palik), Academic Press, Boston **1985**.